J. metamorphic Geol., 2007, **25,** 305–320 doi:10.1111/j.1525-1314.2007.00690.x

Formation of spinel-cordierite-feldspar-glass coronas after garnet in metapelitic xenoliths: reaction modelling and geodynamic implications

A. M. ÁLVAREZ-VALERO,[1]* B. CESARE[1,2] AND L. M. KRIEGSMAN[3]
[1]*Department of Mineralogy and Petrology, University of Padova, Corso Garibaldi, 37, I-35137 Padova, Italy (antoniomiguel.alvarez@dgeo.uhu.es)*
[2]*C.N.R. – Istituto di Geoscienze e Georisorse, Corso Garibaldi, 37, I-35137 Padova, Italy (bernardo.cesare@unipd.it)*
[3]*National Museum of Natural History/Naturalis, PO Box 9517, NL-2300 RA Leiden, The Netherlands (kriegsman@naturalis.nl)*

ABSTRACT Spinel + cordierite + K-feldspar + plagioclase + glass form coronas around garnet in metapelitic xenoliths at El Hoyazo and Mazarrón, two localities of the Neogene Volcanic Province (NVP) of SE Spain. The presence of fresh glass (quenched melt) in all phases shows that corona development occurred under partial melting conditions. Algebraic analysis of mass balance in the NCKFMASH system suggests the reaction Grt + Sil + Bt + Pl = Spl + Crd + Kfs + melt as the most plausible model for the development of coronas in the El Hoyazo sample, and indicates that biotite was required as reactant for the formation of cordierite. The *P–T* conditions for the formation of coronas are estimated at ~820 ± 50 °C, 4.5 ± 0.6 kbar at El Hoyazo, and ~820 ± 50 °C, 4.0 ± 0.4 kbar at Mazarrón. The El Hoyazo xenoliths record a complex *P–T* history, characterized by early melt production during heating and additional melting during decompression. A local cooling event characterized by minor retrograde reaction and melt crystallization preceded ascent and eruption. This study shows that detailed xenolith analysis may be used to track magma evolution in a chamber.

Key words: algebraic analysis; corona; decompression; Neogene Volcanic Province; partial melting.

INTRODUCTION

The mineral assemblage garnet-spinel-cordierite-feldspar-quartz-biotite-sillimanite is typical of metapelitic systems at high temperature (HT) and low (LP) to medium pressure (MP) (e.g. Hand *et al.*, 1994; McDade & Harley, 2001; White *et al.*, 2001, 2002; Cenki *et al.*, 2002; Ings & Owen, 2002; Riesco *et al.*, 2004). Such *P–T* conditions are also propitious for the assemblage to be accompanied by melt, derived by partial melting of the rocks. A typical microstructural feature in these metapelites is the intergrowth of spinel and cordierite, which usually replaces garnet-sillimanite-bearing assemblages (e.g. Mezger *et al.*, 2001; Topuz *et al.*, 2004), and/or andalusite (Cesare *et al.*, 2003a; Johnson *et al.*, 2004). Spinel-cordierite assemblages may occur as coronitic and/or symplectic microstructures, related to particular kinetic conditions of low chemical diffusion rate (Hand *et al.*, 1992; Passchier & Trouw, 1996; Vernon, 1996; Whittington *et al.*, 1998).

A coronitic microstructure, where reactant(s) and product(s) are easily inferred, is one of the most common examples where the stoichiometry of metamorphic reactions can be constrained and balanced. However, in the case of melt-bearing assemblages under anatectic conditions, the evaluation of the role of some phases can be problematic. This is particularly true for the role of the melt itself, as it has commonly recrystallized or left the rock by melt extraction (e.g. McDade & Harley, 2001; White *et al.*, 2001; Cenki *et al.*, 2002; White & Powell, 2002; Riesco *et al.*, 2004). It follows that almost all melt-bearing reactions are modelled using theoretical melt compositions, which do not correspond to a phase that can be analysed in the rock. Exceptions to this rule are where it has been preserved as glass, for example, in crustal xenoliths rapidly quenched during volcanic eruption.

Several xenolith types have been described in the Neogene Volcanic Province (NVP) of SE Spain (Zeck, 1968; Cesare *et al.*, 1997; Álvarez-Valero, 2004), and one of these xenolith groups is represented by Spl-Crd-bearing rocks. Glass, inferred to represent melt, is always present in the NVP samples, suggesting rapid cooling after partial crustal melting at LP granulite facies conditions (Cesare *et al.*, 2003b; Álvarez-Valero *et al.*, 2005). Fast cooling prevented retrograde re-equilibration of the xenoliths (Kriegsman & Hensen, 1998; Kriegsman, 2001) except in rare microstructural cases. Among the Spl-Crd-bearing xenoliths, a few samples show a coronitic reaction in which garnet is separated from the surrounding matrix (which is

**Present address:* Departamento de Geología, Facultad de Ciencias Experimentales, Universidad de Huelva. Campus El Carmen, Avda. Fuerzas Armadas, s/n, 21071, Huelva, Spain.

mainly composed of Fib + Pl) by a corona of Spl + Crd + Kfs + glass (mineral abbreviations after Kretz, 1983; Fib = acicular sillimanite according to the definition of Pattison, 1992; M = melt).

Considering the special nature of these coronas and the presence of fresh glass in them, this study describes the microstructures and the mineral chemistry, balances the reaction stoichiometry of corona development in the NCKFMASH system, and defines the *P–T* evolution of the rocks in the LP domain of the granulite facies.

GEOLOGICAL SETTING

The NVP is located in the Internal Zones or Alborán Domain of the Betic Cordillera in the western Mediterranean (Fig. 1a). The Alborán Sea is a basin which formed by extension starting at *c.* 25 Ma during the Miocene evolution of the Betic Cordillera, which was characterized by the convergence between the African and Eurasian plates. In this region, partial melting appears to have developed in a thinned continental crust after a major phase of lithospheric extension (Platt & Vissers, 1989; Vissers *et al.*, 1995).

The NVP is mainly composed of high-K calcalkaline rocks, mostly andesites and dacites (Fernández-Soler, 1996; Benito *et al.*, 1999). The age of the NVP volcanites ranges from 17 to 5 Ma (Zeck *et al.*, 1998; Turner *et al.*, 1999; Cesare *et al.*, 2003b; Duggen *et al.*, 2004). Some of the high-K calcalkaline lavas, mostly dacites, are Grt-Crd-bearing and crop out as small scattered, volcanic extrusions, aligned within a SW–NE-trending zone that extends for approximately 200 km at the south-eastern margin of Spain.

El Hoyazo is a fossil volcano with around 500 m crater radius and is overlain by Miocene reef carbonates. The lavas include up to 15 vol.% crustal material (Zeck, 1968). The erupted volcanic rocks form $\sim$1 km^2 of surface outcrop. In the proximity of Mazarrón village, several outcrops of volcanic rocks of variable size occur. Lava outcrops are much larger ($\sim$100 km^2) than at El Hoyazo, but typical volcanic morphologies are not developed here. Xenoliths providing evidence for partial melting within the lavas at El Hoyazo and Mazarrón are fine- to medium-grained granulite facies rocks that range in size from a few tens of centimetres down to single xenocrysts. Xenoliths are interpreted to be the result of restite fragmentation and dispersion in the host lava, possibly because of explosive emplacement. They have been characterized and described in detail by Zeck (1968, 1970) at El Hoyazo, and Cesare & Gómez-Pugnaire (2001) at El Hoyazo and Mazarrón. In both areas, two main types of xenoliths were distinguished: Grt-Bt-Sil-dominated and Spl-Crd-dominated. All xenoliths are strongly depleted in silica and enriched in aluminium and iron (Zeck, 1968; Cesare *et al.*, 1997; Benito *et al.*, 1999) with respect to common metapelites (e.g. Taylor & McLennan, 1985). They have been interpreted as the residue following extraction of rhyolitic melt from graphitic metapelites (Cesare *et al.*, 1997).

Zeck (1970), Cesare *et al.* (1997) and Cesare & Gómez-Pugnaire (2001) proposed that the high-K dacitic lava and most of the xenoliths may be interpreted as co-genetic products from the partial melting of graphitic metapelites. However, the anatectic magma has been contaminated with mafic melts (Benito *et al.*, 1999).

Available geothermometric data on the xenoliths of El Hoyazo indicate equilibration at 850 ± 50 °C and $\sim$5.5–7 kbar (Cesare *et al.*, 1997, 2003b), with the same temperature range but lower pressure ($\sim$4 kbar) at Mazarrón (Cesare & Gómez-Pugnaire, 2001). SHRIMP ages obtained from zircon and monazite of the xenoliths and their host dacite indicate that anatexis took place at *c.* 9.7–8.1 Ma at El Hoyazo and 9.1 Ma at Mazarrón, whereas the eruption has been dated at *c.* 6.3 Ma at El Hoyazo and 9.1 Ma at Mazarrón (Zeck & Williams, 2002; Cesare *et al.*, 2003b). Hence, at El Hoyazo, the crustal melt resided for at least 3 Myr at depth, while at Mazarrón the partial melting event was practically coeval with the exhumation (Cesare *et al.*, 2003b).

PETROGRAPHY

General features of the Spl-Crd xenoliths with coronitic microstructures

The xenoliths show a massive aspect, lacking a well-developed foliation, and rarely exceed 20 cm in length. The grain size is generally $<$1 mm, except for garnet and cordierite porphyroblasts, which may exceed 5 mm. The typical phase assemblage is hercynitic spinel, cordierite, biotite, garnet, fibrolite, glass, K-feldspar, plagioclase, ilmenite and graphite. The coronitic Spl-Crd xenoliths at El Hoyazo and Mazarrón commonly show garnet rimmed by spinel + cordierite + K-feldspar + M ± plagioclase coronas overgrowing the matrix, which is composed mainly of a mixture of fibrolite + plagioclase ± glass (Fig. 1b). One of the most striking aspects of many rocks is the large amount of the Pl + Fib-bearing matrix anastomosing around coronitic garnet microstructure, and the omnipresence of glass, as inclusions in solid phases, as thin intragranular films or layers, and as devitrified and/or fresh pockets.

Garnet displays equidimensional shape and resorbed rims, and is generally $<$2 mm in diameter. It locally shows biotite, melt and fibrolite inclusions. At least four microstructural variants of 'cordierite' occur in these samples: (i) cordierite as constituent of the coronas around garnet (Fig. 1b); (ii) cordierite crystals in the matrix, with inclusions of glass, biotite and fibrolite; (iii) mantles of cordierite rimming spinel crystals overgrowing the matrix; and (iv) cordierite in symplectic intergrowths with biotite and plagioclase, which occurs in a few samples.

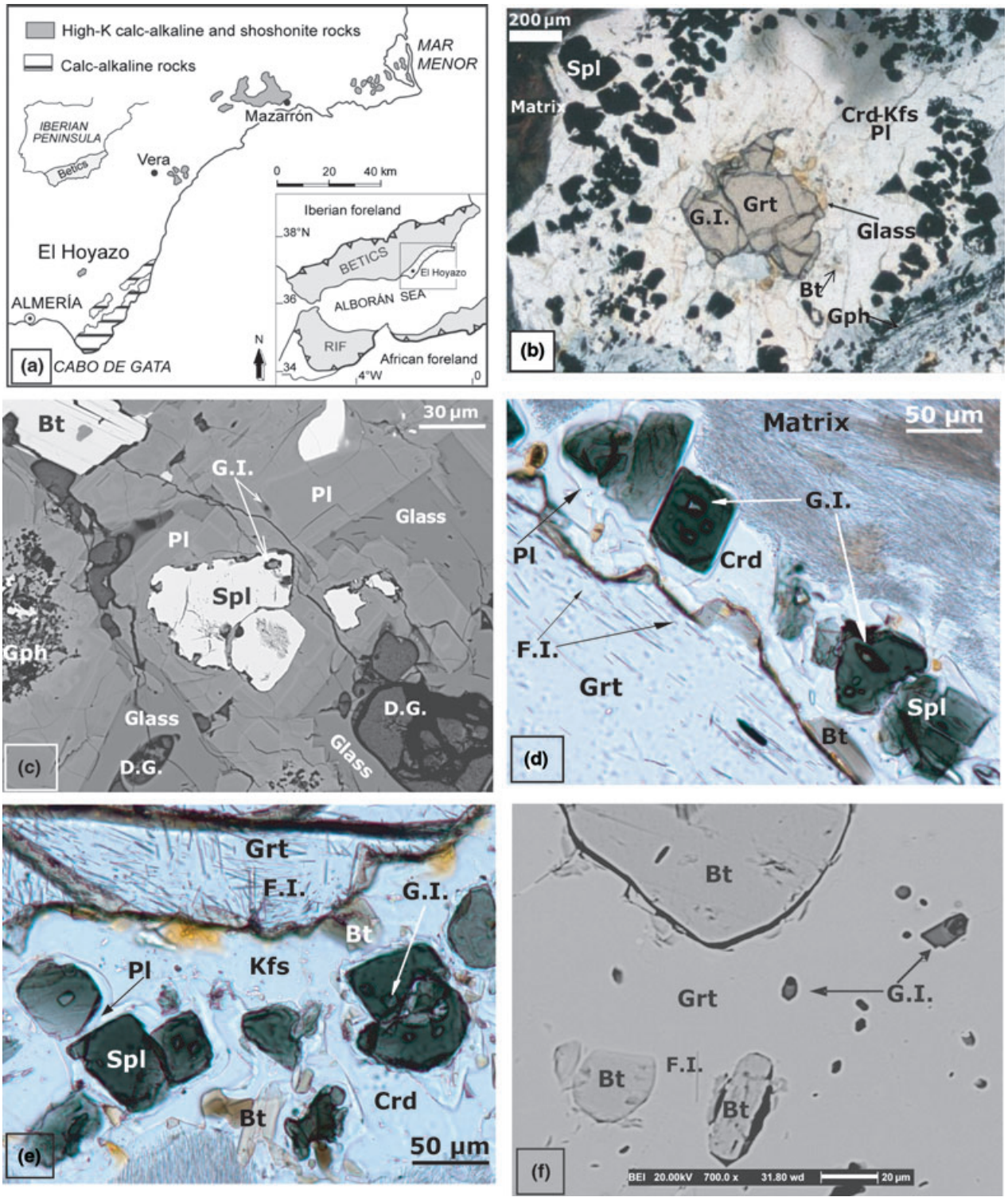

Fig. 1. (a) Geographic location and schematic tectonic elements of the main edifices of the Miocene volcanics of the Neogene Volcanic Province within the Alborán Domain (after López-Ruiz & Rodríguez-Badiola, 1980). (b) Microscopic, plane-polarized light view of a Spl + Crd + Kfs + Pl corona separating garnet from the Sil-Pl-glass matrix at Mazarrón. (c) SEM-BSE view of a spinel with a rim of plagioclase; pockets of fresh and devitrified glass are also visible (G. I. glass inclusions; D. G. devitrified glass). (d), (e) Microscopic, plane-polarized light details of coronas with Spl, which is never in contact with Grt nor with the matrix; Spl crystals show glass inclusions (G. I.) and a thin Pl rim (F. I. fibrolite inclusions). (f) SEM-BSE view of a garnet with biotite and glass inclusions.

Spinel shows two main variants. One occurs within the coronas surrounding garnet together with cordierite + K-feldspar ± glass ± plagioclase ± biotite ± ilmenite (Fig. 1b). Locally, spinel has a thin rim of plagioclase (Fig. 1c). The other spinel variant shows euhedral spinel crystals with a mantle of mainly K-feldspar or cordierite, overprinting the matrix, without any garnet occurring nearby.

K-feldspar forms part of the corona together with mainly cordierite, spinel and glass (Fig. 1b). K-feldspar also occurs mantling euhedral spinels that overgrow the matrix. Some K-feldspar crystals are also present in the matrix.

Plagioclase occurs typically within the matrix (Fig. 1b). It also forms thin rims around spinel within coronas around garnet (Fig. 1c–e). Locally, at El Hoyazo, plagioclase occurs with biotite ± glass ± cordierite in fine-grained aggregates replacing garnet, which probably formed during retrograde reaction. At Mazarrón, the same assemblage forms symplectic intergrowths.

Fibrolitic sillimanite crystals form part of the matrix, and are enclosed by other matrix minerals (e.g. plagioclase and cordierite). Some garnet shows fibrolite inclusions localized at the garnet rim (Fig. 1d,e).

Biotite has variable modes of occurrence in the different samples. In biotite-rich rocks it occurs both as skeletal crystals in the matrix and in the coronitic microstructure as randomly oriented, elongate euhedral crystals. In rare cases, small crystals are enclosed within garnet (Fig. 1f). At Mazarrón, symplectites of biotite-plagioclase-melt and minor cordierite have locally formed after the corona development.

Glass occurs as fresh and devitrified interstitial pockets, and as inclusions mainly in cordierite, spinel, plagioclase and more rarely garnet (Fig. 1c–f). Ilmenite is a minor phase, which appears in the matrix both as small crystals (Fig. 1b) and as larger anhedral crystals related to lenses of biotite. Graphite forms discontinuous layers which define a weak, relict foliation, or as randomly oriented crystals within partly crystallized glass. Graphite is more abundant in biotite-poor samples (Fig. 1b).

Detailed petrography of the coronas

The corona microstructure is composed of a partly to completely resorbed garnet up to 2 mm in diameter which shows a corona of Spl + Crd + Kfs + glass that is only present between garnet and the fibrolite + plagioclase + glass matrix. The corona displays a shell of subhedral spinel within a matrix of cordierite, K-feldspar, plagioclase and glass. Spinel is neither in contact with the matrix nor with garnet (Fig. 1e). In a few cases, spinel in the corona shows a thin rim of plagioclase at the contact with glass (Fig. 1c,e).

The involvement of glass in the microstructure is attested by the melt inclusions in garnet (Fig. 1f), spinel (Fig. 1d,e) and cordierite, and by its former abundance in the matrix (see also Cesare *et al.*, 1997, Fig. 3b). The occurrence of these inclusions as either isolated or small clusters within crystals is strong evidence for their primary origin, i.e. for their entrapment during the growth of the host phases and the formation of the coronas. Therefore, it can be concluded that melt was present throughout the history of garnet formation and its subsequent partial replacement by coronitic phases, until quenching of the xenoliths after eruption.

The ratio between spinel and the other coronitic phases is ~1 (Figs 1b & 2a–e), but the feldspar/cordierite ratio in the corona is variable, possibly reflecting variations of the bulk composition within and among the xenoliths. Figure 3 shows a visualization of phase proportions in the corona. The figure was obtained from algebraic and image manipulation of X-ray elemental maps analysed using SEM. Multichannel images (of Mn, Ti, Fe, Mg, Ca, K, Na, Si, Al) were produced with Adobe Photoshop® and then processed with MultiSpec© (version 3.0). The recognition of phases was performed automatically by cluster analysis followed by the pixel classification routine, using the 'maximum likelihood' method in MultiSpec©. At El Hoyazo, the dominant phase together with spinel is cordierite (Fig. 3a). The example illustrated in Fig. 3b shows a corona richer in K-feldspar than in cordierite.

Several reaction microstructures developed locally after corona development: (i) plagioclase and minor, randomly oriented, euhedral biotite and cordierite crystallized from melt pockets (e.g. in Figs 1c,e & 2a,b); (ii) plagioclase rims around spinel within the corona show well-defined crystal faces and growth zoning; this plagioclase encloses glass and occurs next to pockets of devitrified interstitial melt (Fig. 1c); (iii) symplectic intergrowth of plagioclase and biotite replacing garnet and spinel at Mazarrón (Fig. 2f). These microstructures probably attest to an event of crystallization from cooling glass.

Reaction sequence: microstructural inferences

The petrographic evidence allows inferences on the qualitative role of phases as reactants and products, and thus helps constrain the possible reactions leading to the development of the coronitic microstructures. This preliminary step does not attempt a rigorous mass balance (which follows in a later section). Before corona development, fibrolite inclusions within garnet suggest that during the final stages of garnet growth at expense of a fibrolite-bearing matrix, garnet incorporating fibrolite needles (Fig. 1d,e). Subsequently, both the resorbed aspect of garnet and its Mn-enriched rims suggest garnet consumption. Our interpretation of the microstructure is that the garnet plus corona has replaced a larger, euhedral garnet that was previously in direct contact with fibrolite in the matrix.

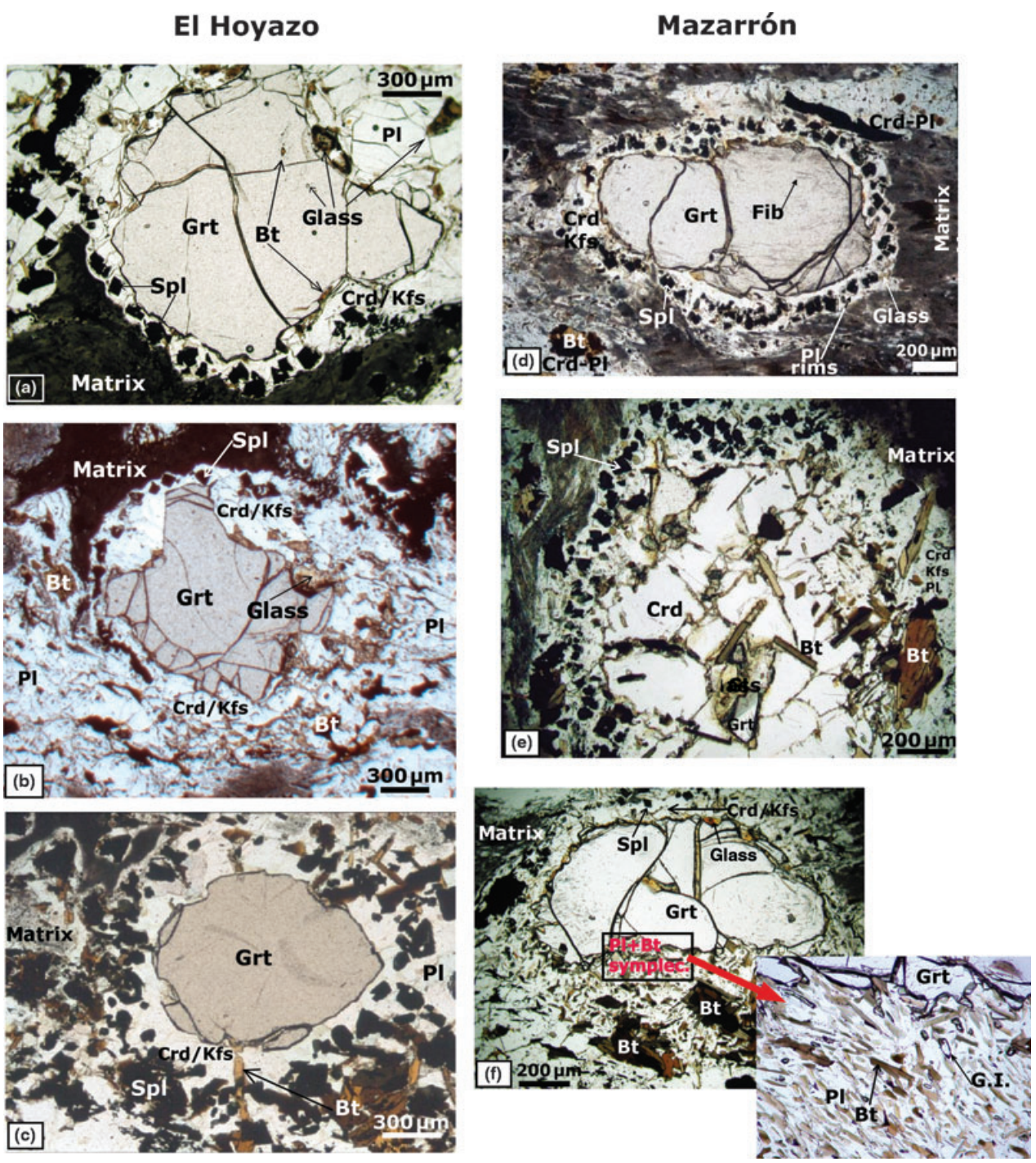

Fig. 2. (a), (b), (c) and (d) Microscopic, plane-polarized light views of Spl + Crd + Kfs + Pl + glass coronas separating garnet from the matrix at El Hoyazo. (e) Corona at Mazarrón, in which garnet is almost completely pseudomorphed by Crd, euhedral Bt and glass. (f) Corona at Mazarrón. The inset shows a symplectic intergrowth of Pl + Bt during a later retrograde reaction event.

Based on the phases observed in the coronas and on their development between garnet and matrix (Figs 1b & 2a–e), a first-order approximation of the prograde melting reaction is:

$$\text{Grt} + \text{Sil}\ (+\text{Pl}) = \text{Spl} + \text{Crd} + \text{Kfs} + \text{M} \qquad (1)$$

The role of plagioclase is uncertain. In reaction (1), it has been considered as a potential reactant because it is a major component of the matrix. However, in some places, plagioclase is present within the coronas, rimming spinel, or growing as euhedral crystals next to

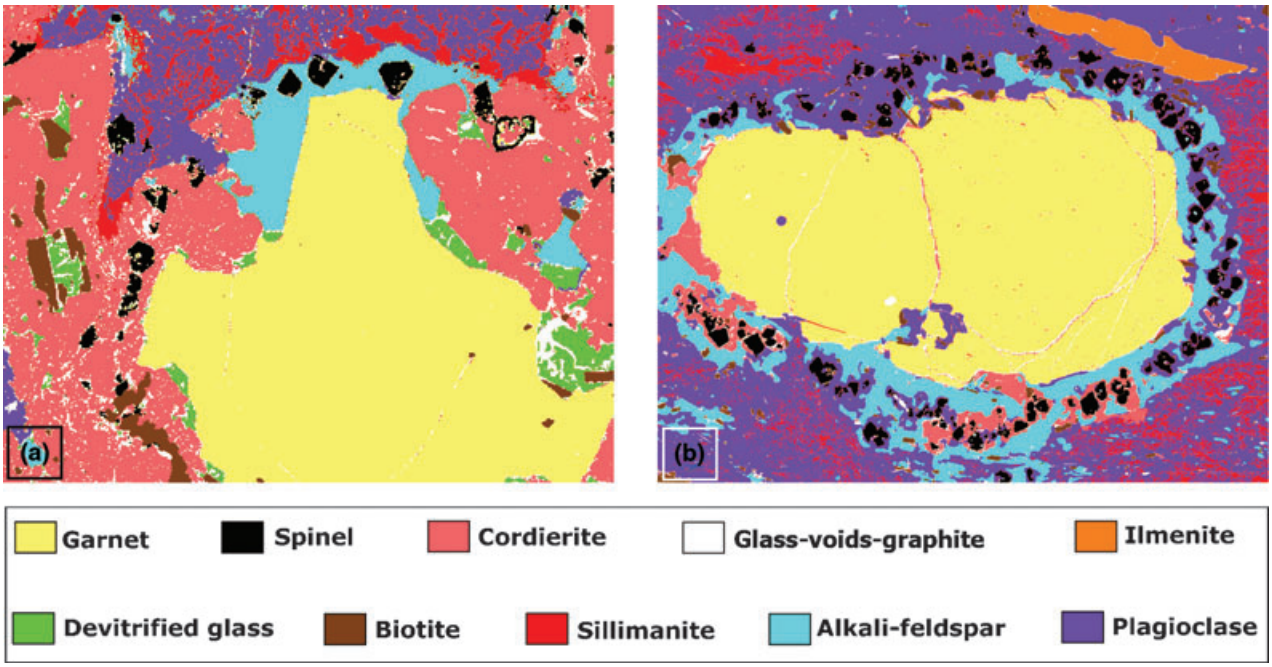

Fig. 3. Phase distribution obtained by manipulation of SEM X-ray maps of Mn, Ti, Fe, Mg, Ca, K, Na, Si, Al. Image analysis produced with Adobe Photoshop® and then processed with MultiSpec© (version 3.0): (a) El Hoyabo, (b) Mazarrón.

glass pockets (Fig. 1d). This would rather suggest the retrograde reaction:

$$\text{Grt} + \text{Sil} + \text{M} = \text{Crd/Kfs} + \text{Spl} + \text{Pl} \qquad (2)$$

The role of plagioclase needs to be evaluated by mass balance considering the possibility that the reaction is continuous in the NCKFMASH system and may involve two different plagioclase generations, i.e. plagioclase_1 (reactant) and plagioclase_2 (product).

Concerning the role of melt, as glass occurs not only as inclusions mainly in garnet, cordierite, spinel and plagioclase, but also as interstitial pockets within the corona, it can be concluded that melt was already present in the rock before corona development, and continued to be present after. This does not imply that melt was necessarily a product of the coronitic reaction. Biotite has been observed as inclusions in garnet (Fig. 1f) and may occur in the matrix surrounding the garnet. Therefore, it can be a potential reactant, as in the modified reaction:

$$\text{Grt} + \text{Sil} + \text{Bt} = \text{Spl} + \text{Crd/Kfs} + \text{M} \qquad (3)$$

If this reaction operated, the scarcity or lack of biotite in a few samples of El Hoyazo and Mazarrón could indicate that biotite was totally consumed during the progress of the reaction. Garnet breakdown was probably halted by kinetic factors. Once the garnet and the matrix were too far apart, they could not react further because diffusion of species was not efficient enough. The distances between spinel and matrix are rather constant and the thickness of the spinel 'shell' is 100–300 μm. Garnet may show not only minor replacement, but also may be completely pseudomorphed. In the latter case, the original garnet size was smaller and the microstructure contains a core of cordierite and spinel in the intermediate part of the corona. The Spl/(Crd + Kfs + Pl + glass) volume ratios observed in the microstructures are typically constant and independent of the extent of garnet replacement, which strongly suggests that all these phases are products of the corona-forming reaction.

A few samples from El Hoyazo and Mazarrón record microstructures that are interpreted to post-date corona formation. The most obvious microstructure is represented by a new generation of biotite, plagioclase and variable amounts of cordierite in symplectic intergrowths replacing garnet at Mazarrón (Fig. 2f). Similar microstructures at El Hoyazo show aggregates of biotite, plagioclase and minor cordierite next to garnet (e.g. in Fig. 2a,b). In both suites, the retrograde reaction can be modelled as:

$$\text{Grt} + \text{Spl} + \text{M} = \text{Bt} + \text{Pl}(\pm\text{Crd}) \qquad (4)$$

These biotite-forming microstructures can be interpreted as products of retrograde melt-consuming reactions related to cooling (Kriegsman & Hensen, 1998; Kriegsman, 2001).

In view of the persistence of undevitrified glass in the matrix surrounding the above microstructures, their origin is likely to reflect minor cooling at supersolidus conditions, lasting long enough to allow crystal growth. Conversely, the thin plagioclase rims around spinel (Fig. 1c–e), with stepped crystal faces towards glass, suggest rapid growth at large degrees of undercooling

Table 1. Representative electron microprobe analyses of minerals at El Hoyazo.

	1 Grt	2 Grt	3 Grt	4 Bt	5 Bt	6 Crd	7 Crd	8 Crd	9 Kfs	10 Pl	11 Pl	12 Pl	13 Hc	14 Hc	15 glass	16 glass	17 glass	18 glass	19 Ilm
SiO_2	37.18	36.96	37.67	34.38	34.17	47.27	48.50	48.44	65.36	57.29	56.01	54.58	0.05	0.06	69.49	72.38	72.88	74.11	0.00
TiO_2	0.04	0.01	0.03	4.82	5.41	0.00	0.01	0.00	0.00	0.00	0.03	0.03	0.24	0.19	0.11	0.10	0.20	0.01	53.65
Al_2O_3	20.66	20.89	21.06	16.38	16.17	31.95	32.32	32.54	18.63	26.75	28.33	28.74	56.36	57.90	13.47	12.88	14.08	12.48	0.17
Cr_2O_3	0.00	0.04	0.02	0.13	0.25	0.00	0.00	0.00	0.02	0.00	0.00	0.00	0.15	0.48	0.00	0.08	0.00	0.00	0.06
FeO	36.79	37.90	34.49	23.29	22.47	12.58	12.41	11.99	0.09	0.06	0.16	0.21	39.16	34.99	2.13	1.49	2.10	1.22	44.71
MnO	1.73	0.40	2.27	0.17	0.13	0.29	0.24	0.01	0.00	0.03	0.07	0.02	0.33	0.39	0.00	0.00	0.00	0.04	0.80
MgO	2.82	2.93	4.14	7.27	7.87	5.95	5.69	6.34	0.00	0.00	0.02	0.02	2.73	4.31	0.00	0.02	0.04	0.14	0.40
CaO	0.87	1.22	1.24	0.04	0.03	0.04	0.06	0.06	0.12	9.02	10.17	11.62	0.00	0.00	0.83	0.78	0.49	0.45	0.00
Na_2O	0.01	0.02	0.00	0.28	0.32	0.03	0.13	0.12	1.88	5.99	5.32	4.74	0.00	0.00	2.79	2.70	1.27	1.81	0.00
K_2O	0.00	0.00	0.05	8.86	9.12	0.13	0.06	0.08	13.55	0.82	0.54	0.45	0.00	0.00	5.30	5.10	3.89	4.15	0.02
NiO													0.00	0.03					
V_2O_5													0.19	0.22					
ZnO													0.45	0.93					
Total	100.11	100.37	100.96	95.63	95.93	99.25	99.43	99.60	99.65	99.96	100.65	100.41	99.67	99.50	94.11	95.52	94.95	94.42	99.80
		(24 Ox)		(11 Ox)			(18 Ox)			(8 Ox)			(4 Ox)						(3 Ox)
Si	6.011	5.950	5.977	2.738	2.714	4.981	5.033	5.007	2.999	2.575	2.506	2.459	0.002	0.002					0.000
Ti	0.004	0.002	0.003	0.289	0.323	0.000	0.967	0.993	0.000	0.000	*0.001*	0.001	0.005	0.004					1.018
Al	*3.939*	*3.966*	3.938	1.540	1.520	3.968	3.953	3.965	1.008	1.418	1.494	1.526	1.925	1.944					0.005
Cr	0.000	0.002	0.001	0.008	0.016	0.000	0.001	0.000	0.001	0.000	0.000	0.000	0.003	0.011					0.001
Fe^{2+}	4.975	5.103	4.576	1.514	1.454	1.108	1.077	1.036	0.003	0.002	0.006	0.008	0.949	0.834					0.943
Mn	0.237	0.055	0.305	0.012	0.009	0.026	0.021	0.001	0.000	0.001	0.002	0.001	0.008	0.009					0.017
Mg	0.680	0.703	0.979	0.863	0.931	0.935	0.880	0.976	0.000	0.000	0.002	0.001	0.118	0.183					0.015
Ca	0.151	0.210	0.210	0.003	0.003	0.005	0.007	0.007	0.006	0.435	0.488	0.561	0.000	0.000					0.000
Na	0.000	0.000	0.000	0.044	0.049	0.006	0.026	0.025	0.167	0.522	0.461	0.414	0.000	0.000					0.000
K	0.001	0.004	0.009	0.900	0.924	0.018	0.009	0.011	0.793	0.047	0.031	0.026	0.000	0.000					0.001
X_{Mg}	0.12	0.12	0.18	0.36	0.39	0.46	0.45	0.49					0.11	0.18					0.02
Alm	0.82	0.84	0.75					X_{Ab}	0.17	0.52	0.47	0.41 Zn	0.01	0.02 ASI	1.5	1.5	2.5	1.9 X_{Ilm}	0.94
Sps	0.04	0.01	0.05					X_{An}	0.01	0.43	0.50	0.56 V	0.00	0.00				X_{Hem}	0.02
Gr	0.02	0.03	0.03					X_{Or}	0.82	0.05	0.03	0.03 Ni	0.00	0.00					
Prp	0.11	0.12	0.16																

1 = Grt core; 2 = Grt innermost rim; 3 = Grt outermost rim; 4 = Bt in matrix; 5 = Bt within the corona; 6 = Crd around Spl; 7 = Crd in contact with garnet; 8 = Crd in matrix; 9 = Kfs; 10 = Pl in matrix; 11 = Pl rimming Spl within the corona; 12 = Pl (retrograde); 13 = Hc core; 14 = Hc rim; 15, 16 = glass inclusions (G.I.) in Spl; 17 = G.I. in Pl; 18 = glass interstitial; 19 = Ilm. $X_{mg} = Mg/(Fe^{2+} + Mg)$, $X_{Ab} = Na/(Ca + Na + K)$, $X_{An} = Ca/(Ca + Na + K)$, $X_{Or} = K/(Ca + Na + K)$, $X_{Ilm} = Fe^{2+}$, $X_{Hem} = 1 - (Fe^{2+} + Mg + Mn)$.
Mineral formulae based on the number of oxygen as in brackets. All iron as FeO.

(see Vernon, 2004), and are compatible with minor crystallization of the interstitial melt during quenching after eruption.

MINERAL CHEMISTRY

Two samples were selected for the chemical study of the coronitic microstructures: HZ-X for El Hoyazo (Table 1) and AV-Ma 8.7 for Mazarrón (Table 2). All phases including glass were analysed using a Cameca Camebax electron microprobe (EMP) at the Consiglio Nazionale delle Ricerche (C.N.R.), Department of Mineralogy and Petrology, University of Padova. Natural and synthetic silicates and oxides were used as standards, and data correction was performed using PAP methods (Pouchou & Pichoir, 1984). Working conditions were 15 kV accelerating voltage and 15 nA sample current. The beam diameter was generally focused to ~1 μm for solid phases, but was defocused to ~5–10 μm for glass analysis. Despite the defocused beam, alkali loss is almost unavoidable in the glass analyses, and the analytical setup recommended by Morgan & London (1996) could not be used.

X-ray elemental maps were obtained with a Camscan MX2500 equipped with a tungsten cathode, a four-quadrant solid-state BSE detector and an EDX-EDAX system for microanalysis. The analytical conditions were: accelerating voltage – 20kV; filament emission – 160 nA; working distance – 35 mm; matrix size for the X-ray maps – 512 × 400 pixels, with a duration of around 12 h.

El Hoyazo

Resorbed garnet is an almandine-rich solution in the range $Alm_{75-84}Prp_{10-16}Sps_{0-6}Grs_{2-4}$ (Table 1). As apparent from Fig. 4a,b, garnet preserves a bell-shaped Mn zoning pattern, with MnO = 2.5 wt% at the core decreasing to 0.2 wt% at the inner rim. The outermost rim, for ~30 μm, shows an abrupt increase from inner ring values in MnO up to 2.2 wt%. This Mn pattern is opposite to slight variations in X_{Mg} that rise from low values in the core (0.11–0.14) to maximum values (0.18) at the outermost rims.

The MnO patterns of these garnet can be interpreted as a primary growth zoning followed by an event of garnet resorption with selective incorporation of Mn within the progressively disssolving rims (e.g. Hollister, 1977). In this case, because of replacement by cordierite and melt, preserved in glass inclusions, the Mn pattern is not related to a retrograde event, such as in the example modelled by Storm & Spear (2005). The Mn contents of cordierite in the coronas also support this conclusion.

Table 2. Representative electron microprobe analyses of minerals at Mazarrón.

	1 Grt	2 Grt	3 Grt	4 Bt	5 Bt	6 Crd	7 Crd	8 Crd	9 Kfs	10 Pl	11 Pl	12 Pl	13 Hc	14 Hc	15 glass	16 glass	17 glass	18 glass	19 Ilm
SiO_2	37.62	37.41	37.92	35.10	34.96	48.18	48.40	49.11	62.67	51.23	56.22	54.84	0.00	0.07	70.92	70.99	72.80	71.60	0.00
TiO_2	0.06	0.00	0.02	5.25	0.85	0.02	0.00	0.06	0.00	0.00	0.01	0.02	0.02	0.04	0.04	0.16	0.02	0.09	52.28
Al_2O_3	21.09	20.75	20.92	16.44	18.47	32.75	32.45	32.71	19.02	31.02	27.42	28.58	58.41	57.30	14.16	15.05	14.25	13.48	0.08
Cr_2O_3	0.00	0.01	0.08	0.17	0.09	0.00	0.00	0.03	0.02	0.00	0.00	0.04	0.11	0.22	0.02	0.05	0.00	0.04	0.00
FeO	37.18	37.06	34.23	21.68	21.50	11.29	12.82	9.09	0.32	0.13	0.30	0.17	35.99	35.98	1.81	2.31	1.94	1.83	46.02
MnO	0.57	0.62	2.63	0.19	0.20	0.37	0.19	0.25	0.03	0.02	0.04	0.01	0.30	0.25	0.09	0.07	0.05	0.04	0.61
MgO	3.63	3.77	3.51	8.34	9.03	6.50	6.03	8.00	0.00	0.00	0.00	0.00	3.90	3.94	0.08	0.04	0.07	0.09	0.46
CaO	1.20	1.27	1.29	0.00	0.07	0.09	0.06	0.03	0.20	14.69	9.85	11.38	0.00	0.00	1.25	1.03	0.57	0.86	0.00
Na_2O	0.00	0.00	0.00	0.27	0.38	0.12	0.03	0.04	2.12	3.46	5.66	4.76	0.00	0.00	1.02	1.52	1.40	1.15	0.00
K_2O	0.02	0.01	0.03	8.77	9.11	0.19	0.15	0.17	12.51	0.25	0.51	0.34	0.00	0.00	5.15	5.05	5.32	3.54	0.01
NiO													0.00	0.04					
V_2O_5													0.10	0.26					
ZnO													1.10	0.90					
Total	101.38	100.90	100.62	96.21	94.66	99.52	100.14	99.48	96.89	100.79	100.02	100.14	99.94	99.00	94.54	96.28	96.42	92.72	99.47
		(24 Ox)		(11 Ox)			(18 Ox)			(8 Ox)			(4 Ox)						(3 Ox)
Si	5.969	5.962	6.058	2.752	2.748	4.980	5.000	5.020	2.964	2.319	2.532	2.472	0.000	0.002					0.000
Ti	0.007	0.000	0.003	0.309	0.051	0.000	0.000	0.010	0.000	0.000	0.000	0.001	0.000	0.001					0.994
Al	*3.945*	*3.899*	*3.940*	1.520	1.710	3.990	3.952	3.940	1.051	1.656	1.456	1.519	1.947	1.931					0.002
Cr	0.000	0.001	0.005	0.010	0.005	0.002	0.000	0.002	0.001	0.000	0.000	0.000	0.003	0.005					0.963
Fe^{2+}	4.934	4.939	4.573	1.386	1.394	0.976	1.108	0.777	0.011	0.005	0.011	0.007	0.851	0.860					0.013
Mn	0.076	0.084	0.355	0.013	0.013	0.033	0.016	0.022	0.000	0.001	0.002	0.000	0.007	0.006					0.017
Mg	0.859	0.896	0.835	0.974	1.058	1.002	0.928	1.219	0.000	0.000	0.000	0.000	0.164	0.168					0.000
Ca	0.204	0.216	0.220	0.000	0.006	0.010	0.006	0.003	0.014	0.713	0.476	0.550	0.000	0.000					0.000
Na	0.001	0.001	0.000	0.042	0.058	0.025	0.007	0.007	0.171	0.304	0.494	0.416	0.000	0.000					0.000
K	0.001	0.001	0.006	0.877	0.914	0.025	0.02	0.022	0.768	0.014	0.029	0.020	0.000	0.000					
X_{Mg}	0.15	0.15	0.15	0.41	0.43	0.51	0.46	0.61					0.18	0.18					0.01
Alm	0.81	0.80	0.76					X_{Ab}	0.18	0.29	0.49	0.42 Zn	0.02	0.02 ASI	1.9	2.0	2.0	2.4 X_{Ilm}	0.96
Sps	0.01	0.01	0.06					X_{An}	0.01	0.69	0.48	0.56 V	0.00	0.00				X_{Hem}	0.01
Gr	0.03	0.04	0.04					X_{Or}	0.81	0.01	0.03	0.02 Ni	0.00	0.00					
Prp	0.14	0.15	0.14																

Numbers and procedure as in Table 1, except 15 = G.I. in Crd.

Biotite has high TiO_2 contents, ranging from 3.9 to 6.4 wt%, with no systematic relation to the microstructural settings in which it occurs. X_{Mg} generally ranges from 0.33 to 0.42, although values as low as 0.24 occur. The F and Cl content are <0.5 and <1.1 wt% respectively.

Cordierite has variable X_{Mg} values in the range 0.25–0.50 as a function of its microstructural setting. The highest X_{Mg} values correspond to euhedral crystals associated with retrograde biotite. The average EMP total of cordierite is >99.3, indicating low volatile contents. Adjacent to garnet with bell-shaped Mn profiles (e.g. Fig. 4b), some cordierite display a slight MnO zoning, with contents falling from the garnet contact towards the matrix, suggesting that cordierite inherited the Mn pattern while replacing garnet.

Spinel is a hercynite-rich solid solution that has compositions in the range $Hc_{74-88}Spl_{8-21}Gah_{<4}$. The range of X_{Mg} (0.08–0.20) does not vary systematically as a function of the microstructural setting, essentially reflecting variations between grains in the same corona. The ZnO content of the spinel crystals within the corona is <1.1 wt%, without significant intracrystalline zoning.

Plagioclase crystals at El Hoyazo show a compositional range from An_{40} to An_{57}, $Or_{<5}$. The highest An values typically correspond to coronitic and retrograde plagioclase crystals, and the lowest to the plagioclase associated with fibrolite in the matrix.

Alkali-feldspar crystals have composition in the range $Or_{80-84}Ab_{16-19}An_{<1}$. Glass from fresh interstitial melt pockets and as inclusions has a peraluminous rhyolitic composition. The total wt% (93–97) for both microstructural settings suggests hydrous conditions, even if some loss of Na during analysis is taken into account. Glass inclusions show slightly higher FeO contents (1.5–2.2 wt%) and lower equilibrium ASI [ASI = mol. $Al_2O_3/(CaO + Na_2O + K_2O)$] values (1.5–1.8), than the fresh interstitial glass pockets (FeO = 1.0–1.9 wt%; ASI = 1.8–3.0). Ilmenite has a rather constant composition, with $X_{Ilm} = 0.93$–0.96.

Mazarrón

Unlike at El Hoyazo, garnet cores have a flat compositional pattern until the outermost 40 μm, where the most significant change is the abrupt rise of MnO from 0.5–1.6 wt% to 3 wt% (Fig. 4c,d; Table 2). The overall compositional range is $Alm_{74-82}Prp_{11-16}Sps_{1-9}Grs_{3-4}$ and $X_{Mg} = 0.12$–0.18. The Mn zoning pattern can be interpreted as the result of a stage of flattening of the bell-shaped profile after or during growth. Similar to samples from El Hoyazo, selective incorporation of Mn at the rim occurred by an event of garnet resorption.

Biotite has wide TiO_2 compositional variation from 0.7 to 5.3 wt%. This variability is related to microstructural location. The highest Ti values correspond to biotite enclosed by garnet and to

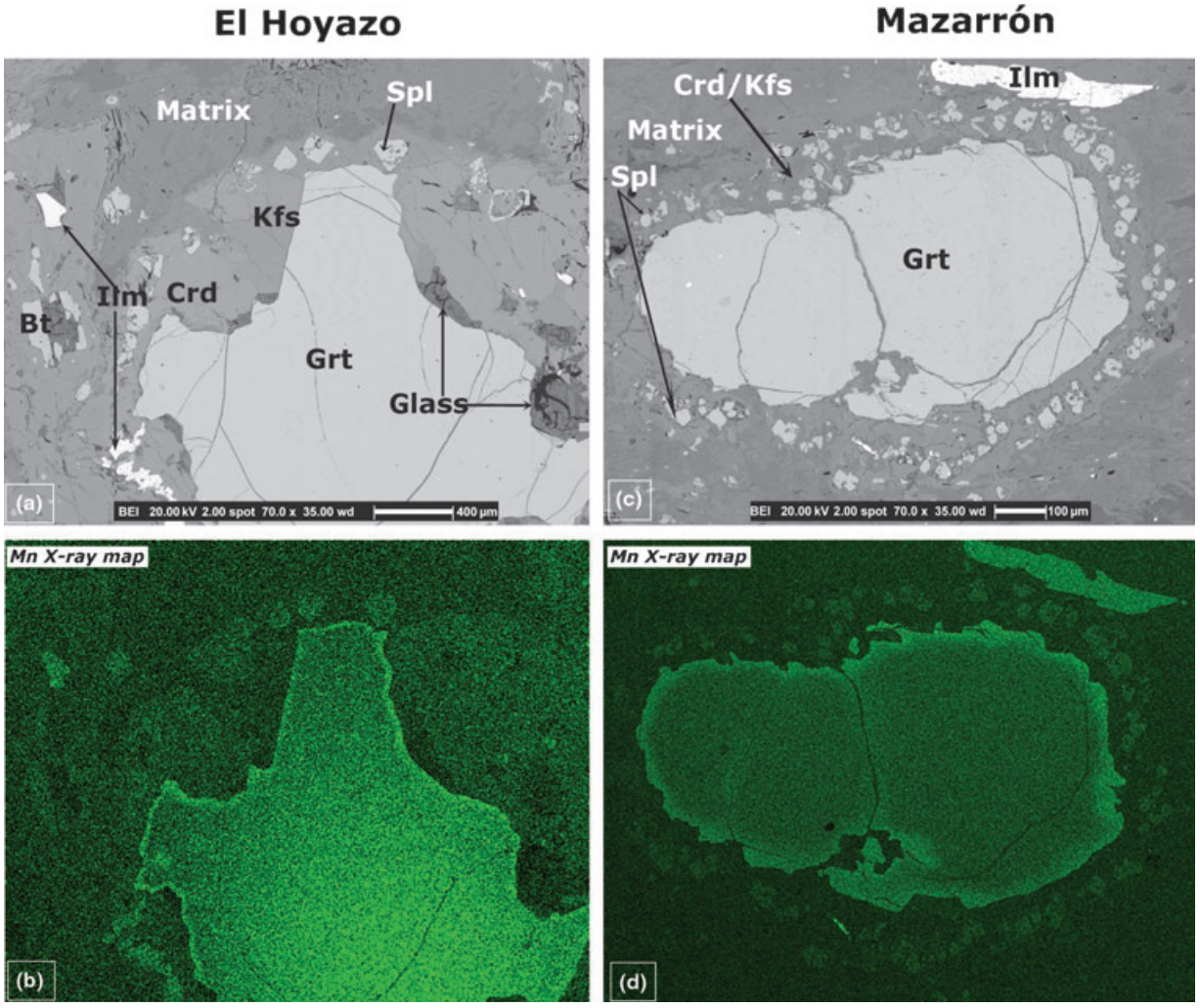

Fig. 4. SEM-BSE images and Mn X-ray maps of garnet rimmed by Spl + Crd + Kfs overprinting the matrix from El Hoyazo (a, b; same area as Fig. 3a) and Mazarrón (c, d; same area as Fig. 3b). Note in (b) and (d) the resorbed high-Mn garnet borders.

crystals within the matrix associated with ilmenite. The lowest TiO_2 values belong to the interpreted late or retrograde biotite, i.e. euhedral crystals within the corona, and those forming symplectites with plagioclase and cordierite. However, X_{Mg} values (0.25–0.45) lack a systematic relationship to the microstructural setting.

Cordierite is again volatile-poor, with average EMP totals >99.5. X_{Mg} ranges from 0.42 to 0.69. Coronitic cordierite has lower X_{Mg} than matrix cordierite. The highest X_{Mg} values belong to euhedral crystals in contact with retrograde biotite.

Spinel composition shows minor compositional variations in the range of $Hc_{76-83}Spl_{13-17}Gah_{<5}$, without any systematic correlation with the microstructural location of crystals. The composition of plagioclase varies from An_{42} to An_{81}, $Or_{<4}$. The highest An values belong to retrograde plagioclase crystals, those in the matrix and within the symplectitic microstructure with biotite.

Alkali-feldspar is $Or_{79-81}Ab_{18-20}An_{<2}$. Glass as both fresh interstitial glass pockets and inclusions is characterized by a peraluminous rhyolitic composition. For both microstructural settings, the EMP totals (93–98 wt.%) suggest hydrous conditions, even when considering some loss of Na during analysis. The ASI values are normally higher for fresh interstitial glass pockets (2.4) than for glass inclusions (1.7–2.0). FeO content for both microstructural contexts is similar (1.8–2.3 wt%). Ilmenite has rather constant composition, with $X_{Ilm} = 0.93$–0.96.

ALGEBRAIC MASS BALANCE ANALYSIS

Method and assumptions

The detailed mineral chemical data available allow use of linear algebra to investigate the compositional space of the corona microstructures and their host rocks, with the aim of balancing the reaction that led to

corona development. Investigation of compositional matrices to examine linear dependencies between minerals (Greenwood, 1967) has been performed using the C-Space software (Torres-Roldán *et al.*, 2000). This method of analysis has recently been reviewed by Day & Springer (2005). The evaluation of possible reaction relationships within a compositional matrix, and the problems related to it, have been discussed by Fisher (1989) and Cesare (1999).

By definition, in a compositional matrix, solutions can be obtained only when the number of phases (P) is greater than the number of components (C), and as each solution contains $C + 1$ phases, the choice of the input data turns out to be the main controlling factor of the calculation. In the samples from El Hoyazo, as a result of the microstructural and microchemical investigation, corona development was modelled using 10 phases: Bt, Crd, Grt, Sil, Spl, Kfs, Pl_1, Pl_2, melt and fluid. Input biotite is Ti-rich as is expected for a reactant close to its maximum thermal stability; garnet composition corresponds to the inner rim, low in MnO; spinel composition is an average of core–rim variations, with intermediate X_{Mg}; cordierite corresponds to a high X_{Mg} term, as found in the coronas; melt composition is from a glass inclusion in cordierite trapped during corona development; fluid is pure H_2O. Pl_1 is more sodic (An_{43}), as the one occurring in the matrix, associated with fibrolite, Pl_2 is more calcic (An_{56}), and corresponds to the crystals associated with spinel in the coronas.

The use of two compositions for plagioclase was considered, as microstructurally they evidence two different generations, and as it allows the possibility of detecting continuous variations during reactions (e.g. Hartel & Pattison, 1996). Other phases in the rock (e.g. garnet, spinel, melt) show significant compositional variations, but addition of phases at a constant number of components results in a much greater number of univariant relations with little petrological significance. However, we have also tested compositional matrices with two garnet or two melt compositions, and their results are similar to those of the compositional matrix analysed in detail here.

The components used in the input matrix are, expressed in wt% as from EMP results (with the exception of H_2O): Na_2O, CaO, K_2O, FeO, MgO, Al_2O_3, SiO_2 and H_2O. TiO_2 was omitted, despite being a major component of biotite, because it can be easily balanced by addition of ilmenite as a phase. H_2O was not analysed in minerals and glass, and has therefore been assumed as the difference of EMP total to 100%. This method of inferring water contents should be used very carefully, as EMP totals could be affected by missing components or analytical errors. Although the used H_2O values (2.10, 0.20 & 5.90 for biotite, cordierite and melt, respectively) are reasonable for anatectic metapelites (Harley & Carrington, 2001; Cesare *et al.*, 2003c), we are aware that these are the least constrained parameters of the calculation, and that they could be significantly different, inducing significant changes in mass-balance stoichiometries and petrological inferences. For example, the involvement of K-feldspar as a product or reactant depends critically on the relative H_2O contents of biotite, cordierite and melt (Carrington & Watt, 1995).

Results of El Hoyazo

The resulting input matrix, reported in Table 3a, provides 10 mass balances containing nine phases, which are reported in Table 3b with the missing phases in brackets.

Although all relations in Table 3b are algebraically possible, they are relevant to the formation of coronas only if they satisfy the following conditions: (i) garnet as a reactant; (ii) spinel and cordierite as products. This constraint automatically eliminates mass balances no. 2 to 5 (missing Sil, Grt, Spl and Crd, respectively).

Of the remaining relations, three (no. 7–9) are H_2O-producing, two are H_2O-consuming (no. 1 & 6) and one (no. 10) is fluid-absent. All the H_2O-producing relations have the general form Bt + Grt + Sil + Pl/M = Spl + Crd + Kfs + Pl + H_2O, but their stoichiometries are very different, especially in terms of the Spl/Grt ratio which varies from 1.5 to 22. These mass balances also consume melt (when present). These relations, although mathematically correct, are of poor petrological relevance, as the occurrence of melt inclusions and the absence of fluid inclusions suggest that the role of melt and fluid was the opposite in the formation of coronas.

The Bt-absent mass balance n.1 has the form: Grt + Sil + Kfs + Pl_1 + H_2O = Spl + Crd + Pl_2 + M. Although the two plagioclases are present in the expected position (the An-richer as a product), K-feldspar is a reactant. This is in contradiction with the microstructural evidence of K-feldspar production. It follows that biotite is a necessary reactant in the development of the coronas.

The Kfs-absent mass balance no. 6 has the form: Grt + Sil + Bt + Pl_1 + H_2O = Spl + Crd + Pl_2 + M. Similar to no. 1 but with biotite instead of K-feldspar, this relation also involves plagioclase in the predictable role, and produces a significant mass of melt. However, it lacks K-feldspar. In addition, inspection of its coefficients indicates that it involves a mass of free fluid five times greater than that provided by reacting biotite. This amount of fluid would require porosities in excess of 5 vol.%, which is probably an unrealistic value, even considering the uncertainties in the H_2O contents used in the matrix.

The presence of a fluid-absent mass balance (no. 10) allows investigation of a possible dehydration melting reaction in the formation of coronas. This relationship has the form: Grt + Sil + Bt + Pl_1 = Spl + Crd + Kfs + Pl_2 + M. As it produces all the phases occurring around garnet (Spl, Crd, Kfs and glass), it appears the most appropriate model for corona

Table 3. (a) Input matrix (eight components, 10 phases) with phase compositions (wt%) used for the mass balance calculations of the coronitic reaction at El Hoyazo, and (b) results of the mass balance analysis.

	1	2	3	4	5	6	7	8	9	10
	Bt	Sil	Grt	Spl	Crd	Kfs	Pl_1	Pl_2	glass	fluid
(a)										
SiO_2	33.49	37.00	37.36	0.07	48.46	64.40	57.29	54.35	69.49	0.00
Al_2O_3	17.32	63.00	20.88	56.87	32.82	18.64	26.75	28.92	13.47	0.00
FeO	23.08	0.00	36.17	39.35	11.84	0.15	0.06	0.21	2.13	0.00
MgO	6.34	0.00	3.30	2.52	6.36	0.01	0.00	0.00	0.00	0.00
CaO	0.03	0.00	1.19	0.00	0.03	0.07	9.02	11.53	0.83	0.00
Na_2O	0.36	0.00	0.01	0.00	0.10	1.92	5.99	4.73	2.79	0.00
K_2O	9.21	0.00	0.00	0.00	0.05	13.13	0.82	0.41	5.30	0.00
H_2O	2.10	0.00	0.00	0.00	0.20	0.00	0.00	0.00	5.90	100.00

(b)

1) 15.5 Sil + 28.5 Grt + 15.4 Kfs + 38.1 Pl_1 + 2.5 H_2O = 22.2 Spl + 6.1 Crd + 29.9 Pl_2 + 41.8 M [Bt]
2) 18.6 Bt + 10.7 Spl + 24.0 Pl_2 + 46.7 M = 22.8 Grt + 11.1 Crd + 30.9 Kfs + 32.0 Pl_1 + 3.1 H_2O [Sil]
3) 41.5 Bt + 27.5 Sil + 0.7 Pl_2 + 30.2 M = 15.6 Spl + 36.2 Crd + 42.0 Kfs + 3.5 Pl_1 + 2.7 H_2O [Grt]
4) 30.0 Bt + 12.1 Sil + 15.3 Pl_2 + 42.6 M = 14.4 Grt + 22.8 Crd + 37.9 Kfs + 21.7 Pl_1 + 3.1 H_2O [Spl]
5) 6.9 Bt + 18.8 Spl + 28.9 Pl_2 + 45.3 M = 10.4 Sil + 27.6 Grt + 21.7 Kfs + 37.4 Pl_1 + 2.8 H_2O [Crd]
6) 14.4 Bt + 23.9 Sil + 26.3 Grt + 34.0 Pl_1 + 1.4 H_2O = 26.0 Spl + 18.1 Crd + 27.6 Pl_2 + 28.4 M [Kfs]
7) 41.7 Bt + 29.0 Sil + 2.6 Grt + 26.6 M = 17.7 Spl + 37.0 Crd + 40.9 Kfs + 2.0 Pl_2 + 2.4 H_2O [Pl_1]
8) 41.8 Bt + 28.1 Sil + 0.7 Grt + 29.4 M = 16.3 Spl + 36.6 Crd + 41.9 Kfs + 2.6 Pl_1 + 2.6 H_2O [Pl_2]
9) 33.2 Bt + 31.0 Sil + 16.5 Grt + 19.3 Pl_1 = 25.5 Spl + 32.4 Crd + 24.4 Kfs + 17.0 Pl_2 + 0.6 H_2O [M]
10) 27.4 Bt + 28.9 Sil + 19.7 Grt + 24.0 Pl_1 = 25.8 Spl + 28.0 Crd + 16.7 Kfs + 20.5 Pl_2 + 9.0 M [H_2O]

Note that the univariant balance shows Spl and Crd as products and garnet as reactant. As a function of the C-Space software (Torres-Roldán *et al*., 2000), the absolute rank of input matrix is 8 (up to a computational zero threshold of 1.70367); the possible rank of input matrix is 8 (up to specified zero threshold: 0.0009).
The reaction space matrix is a working set of 10 columns out of 10 in the input model; and null space of the working set has two dimension(s).
The univariant rank of working set reaction is 8 and the working set contains 10 rank + 1 column selections (univariants).

development. Here, as well as in balances no. 1, 6 and 9, the two plagioclases are present on opposite sides with stoichiometric coefficients for reactant Pl_1 greater than for product Pl_2. This suggests that the balance corresponds to a continuous reaction consuming plagioclase and making its composition more An-rich.

Some relevant systematic patterns have emerged from inspection of the compositional space of El Hoyazo sample: (i) in order to have cordierite as product, biotite is required as a reactant; (ii) plagioclase is consumed and becomes more calcic; (iii) K-feldspar is a product. These results need to be taken into account for the modelling of the reaction leading to corona development. For example, they demonstrate that biotite (whose role is not constrained by microstructures) must have been consumed by the reaction.

As a result of the uncertainty in the actual H_2O contents of phases and the presence of minerals with variable composition, the results of the present algebraic analysis should be taken as qualitative. This is in part due to the inability of the algebraic approach to model reactions in multisystems with a large number of phases adequately (i.e. $P \geq C + 2$). Concerning the problems of representativeness of the chosen compositions, when the chemical system was modelled using two garnet compositions (Grt_1, the Mn-poor inner rim and Grt_2, the Mn-rich outer rim), no balances were obtained with Grt_1 as reactant and Grt_2 as product. This implies that the method fails to reproduce the continuous chemical change with Mn increase during garnet consumption, probably because Grt_2 composition is determined by intracrystalline Mn diffusion rather than new growth.

THERMOBAROMETRY

Precise estimation of *P–T* conditions during the formation of the coronas suffers from the problems of thermobarometry in anatectic, Qtz-absent metapelites at low pressure. These are mainly due to the inadequately constrained thermodynamic properties of biotite, cordierite and melt in natural systems, which are in turn strongly dependent on the poorly known behaviour of H_2O in these phases. As a consequence, although the modelling of phase equilibria in the suprasolidus region of metapelitic systems is increasingly performed also in Qtz-absent systems and including components such as Ca, Fe^{3+}, Na and Ti (e.g. White *et al*., 2001, 2003; Cenki *et al*., 2002; Johnson *et al*., 2004; Riesco *et al*., 2004), the results are sometimes different, and in most cases qualitative.

As discussed by Corona-Chávez *et al*. (2006), it may suffice to examine the stability of biotite, which is almost invariably calculated to disappear below 850 °C, whereas it is stable in experiments in excess of 950 °C (e.g. Vielzeuf & Montel, 1994). Although one explanation can be the stabilizing effect of Ti, recently accounted for in thermodynamic databases (White *et al*., 2003), another factor, not yet considered, is the progressive dehydroxylation of biotite. At present, the thermodynamic model adopted for biotite considers a full hydroxyl occupancy (OH = 2), while in nature this constraint is not necessarily true (Cesare *et al*., 2003c).

The uncertainty in the *P–T* position, slopes and stoichiometry of phase boundaries in the LP melting region follows from a comparison of published KFMASH grids (e.g. Cenki *et al.*, 2002; Riesco *et al.*, 2004), where the position of univariant curves may be displaced by > 50 °C. As a result of these uncertainties, along with the arbitrariness of the choice of the chemical subsystem to be modelled (e.g. the amount of biotite to be considered) the choice has been made not to retrieve *P–T* conditions by thermodynamic calculation of pseudosections, but instead to use conventional thermobarometry in comparison with existing petrogenetic grids.

P–T estimates of the coronitic microstructures have been derived from ternary feldspar thermometry, Fe-Mg exchange thermobarometry using Grt-Crd pairs, and net-transfer GASP barometry. The assumption underlying the calculation is that garnet, cordierite and feldspar are in chemical equilibrium. The *P–T* estimates are summarized in Table 4.

At El Hoyazo, using the solvus curves of Nekvasil & Burnham (1987) at the arbitrary pressure of 5 kbar, the feldspar compositions indicate a range of temperatures of crystallization of 778–843 °C. These are cooling, and therefore minimum, temperatures.

A comparable temperature range is given by the Grt-Crd thermometer: 761–863 °C using the calibrations of Thompson (1976) and 728–812 °C with the calibration of Holdaway & Lee (1977). GASP pressure values are highly sensitive to the calibration used: at 800 °C, the pressure ranges from the lower values of 3.1–3.5 kbar of the Koziol (1989) calibration, to the higher limits of 4.4–4.8 kbar of the Koziol & Newton (1988) calibration. It should also be recalled that GASP is strongly sensitive to temperature, and that an increase of 50 °C raises the calculated pressures by > 0.5 kbar. The results of Grt-Crd barometry overlaps with the higher GASP pressures: 3.9–4.5 and 3.9–4.8 kbar with the calibrations of Thompson (1976) and Holdaway & Lee (1977), respectively. Both barometers present the chemical limitation of involving quartz within the equilibrium assemblage. Therefore, as these coronas are quartz-absent, the values obtained must be considered as maxima.

At Mazarrón the temperatures obtained are slightly lower: 771–800 °C using the Grt-Crd calibrations of Thompson (1976) and 736–760 °C with the calibration of Holdaway & Lee (1977). Moreover, the ternary feldspar thermometer gives a lower value of 788 °C. Although at El Hoyazo the Grt-Bt thermometer of Ferry & Spear (1978) and Holdaway (2000) provides results (720–880 °C) overlapping with those of other thermometric methods, at Mazarrón it gives the unrealistic value of 975 °C, suggesting that biotite may not belong anymore to the equilibrium assemblage during the coronitic development process. Calculated pressure conditions at Mazarrón fall in the range 4–5 kbar. Again these are maxima, for a chosen temperature of 800 °C.

Summarizing the results of thermobarometry, the best *T–P* estimates for corona development are ~820 ± 50 °C and 4.5 ± 0.6 kbar at El Hoyazo, and ~820 ± 50 °C and 4.0 ± 0.4 kbar at Mazarrón. The *P–T* conditions for the two xenolith suites at the coronitic stage essentially overlap within the error of the methods. In fact, the coronitic stage at Mazarrón overlaps within error, with the estimates related to the main melting event in the same locality (800 °C and 4.5 kbar; Álvarez-Valero, 2004).

The estimated *P–T* values are in agreement with the phase relations predicted by the KFMASH *P–T* projection and pseudosections for Qtz-absent metapelites of Riesco *et al.* (2004), i.e. they lie within the Crd-Spl-Kfs-melt-stability field at a temperature lower than the formation of Opx + Spl.

Table 4. Summary of the *P–T* calculations obtained for the coronitic microstructure at El Hoyazo and Mazarrón.

Thermometers (°C)	El Hoyazo (at 4.5 kbar)	Mazarrón (at 4 kbar)
Grt-Bt		
Ferry & Spear, 1978	716–872	975
Holdaway, 2000	722–846	943
Grt-Crd		
Thompson, 1976	761–863	771–800
Holdaway & Lee, 1977	728–812	736–760
Two feldspar		
Perchuk *et al.*, 1989	781–802	742
Ternary feldspar		
Nekvasil & Burnham, 1987	778–843	788
Barometers (kbar)	**(at 800 °C)**	**(at 800 °C)**
GASP		
Hodges & Crowley, 1985	3.5–4.2	4.6
Koziol, 1989	3.1–3.5	4.2
Koziol & Newton, 1988	4.4–4.8	5.0
Grt-Crd		
Thompson, 1976	3.9–4.5	4.1–4.3
Holdaway & Lee, 1977	3.9–4.8	4.5–4.5

DISCUSSION

As a result of rapid cooling, the xenoliths preserve fresh glass that can be analysed. This allows a full characterization of the microstructural, chemical and thermobarometric features of the reaction transforming garnet to coronas of spinel, cordierite and K-feldspar.

Because this study deals with small-scale microstructures which are very different from what is usually observed in regionally metamorphosed granulites and which reflect unusually rapid kinetics in an unusual geological setting, one might question its general relevance. We believe, however, that the chemical and thermobarometric constraints are not affected by kinetics and are there fully applicable to other occurrences in HT, LP metapelites. This is supported by comparison with other xenoliths from El Hoyazo and Mazarrón (Cesare *et al.*, 1997; Álvarez-Valero, 2004), where the Spl-Crd-Kfs-Pl-glass assemblage is also development,

but not in coronitic microstructures. These rocks display the same systematic partitioning of elements (in particular Fe and Mg) among phases, and the same ranges of element concentrations as observed in the coronas. Therefore, it appears that chemical equilibrium can be established at a small scale (coronas) before coarsening or annealing of microstructures (other xenoliths).

The chemical characterization of the sample from El Hoyazo, and the investigation of compositional space, has helped understand the role of biotite and feldspar in the coronitic reaction. Whereas on microstructural grounds these phases could be interpreted as both products and reactants, or, in the case of biotite, as not required for the reaction, the mass balance calculations have shown that: (i) biotite is required as a reactant in order to produce significant amounts of cordierite and glass; (ii) plagioclase is a reactant and simultaneously becomes more calcic, i.e. the reaction is continuous; (iii) K-feldspar is produced during the reaction.

The mass balance calculations in the NCKFMASH system provides a preferred solution to the problem, so we can conclude that the reaction leading to corona development has the (unbalanced) form:

$$\mathrm{Grt} + \mathrm{Sil} + \mathrm{Bt} + \mathrm{Pl}_1 = \mathrm{Spl} + \mathrm{Crd} + \mathrm{Pl}_2 + \mathrm{Kfs} + \mathrm{M} \quad (6)$$

where Pl_1 and Pl_2 are the more sodic and more calcic plagioclase compositions, respectively. Because of the systematically higher coefficients for Pl_1, the reaction can be reduced to the form:

$$\mathrm{Grt} + \mathrm{Sil} + \mathrm{Bt} + \mathrm{Pl} = \mathrm{Spl} + \mathrm{Crd} + \mathrm{Kfs} + \mathrm{M} \quad (7)$$

that is the NCKFMASH variant of reaction (3).

The thermobarometric information provided by the corona assemblages can be integrated in a wider model of the petrological evolution of the xenoliths. Again, we focus on the situation at El Hoyazo, where research has been more intense and information more abundant. At this locality, there is extensive evidence that the first and main melting event in the xenoliths took place at significantly higher pressure (5.5–7 kbar; Cesare *et al.*, 1997, 2003b), leading to the development of the Grt-Bt-Sil ± Crd assemblage and to the penetrative foliation of the rocks (Álvarez-Valero *et al.*, 2005). This syntectonic melting event, which predates the development of the coronas, resulted in complete quartz consumption through melt production and extraction, either by the continuous reaction Bt + Sil + Qtz = Grt + M (Álvarez-Valero, 2004) or by a metastable reaction of the type Chl + Ms + Qtz + Ilm + fluid = Grt + Pl + Sil + Bt + M (Cesare & Maineri, 1999). According to the geochronological data of Cesare *et al.* (2003b), the restitic rocks then resided for *c.* 3 Myr at depth, before lava eruption.

Other microstructures attest to a further event overprinting the main assemblage: these are the mantles around elliptical garnet (Álvarez-Valero *et al.*, 2005) and the Spl-Ilm-melt reaction rims at biotite–sillimanite interfaces (Cesare, 2000). Like the coronas of this study, these microstructures are sporadically observed in a minority of samples, developed under post-kinematic conditions, and are of small scale (a few hundreds of micrometre), suggesting an event of short duration. The elliptical garnet mantles are inferred to have developed at 800–900 °C and the reaction rims on biotite at 900–950 °C, ~5 kbar. Although they are not necessarily related to the same event, one interpretation is that these scattered microstructures recording lower pressures of about 4–5 kbar, including the coronas, represent the effects of a short residence of a small number of xenoliths at shallower depth. Because of their post-kinematic character, the most likely interpretation is that these xenoliths were already trapped in the host dacite, probably in an intermediate magma chamber. Álvarez-Valero *et al.* (2005) estimated that the mantle around elliptical garnet formed < 10 000 years before eruption. This would represent the residence time of lava in the magma chamber at 15–19 km (4–5 kbar) depth.

The coronitic microstructures of this study provide further details on this short event of reaction at shallower depth. Figure 3d shows that garnet core and rim have not chemically homogenized with each other, as testified by the sharp chemical change. Considering Mn diffusion coefficients in garnet (Chakraborty & Ganguly, 1991), at a temperature of 850 °C it should take only 1000 years to homogenize the < 30 μm thin external garnet rim of Fig. 3d. Therefore, after residence at high temperature for about 0.5–3.0 Myr after the earlier melting stage, a small fraction of the lava and its xenoliths rose at a shallower depth where it stopped for a maximum of 1000 years during which the garnet reacted and the coronas developed. Without enough time, the homogenization of the sharp change of Mn zoning between core and rim was prevented.

The *P–T* history of the samples of El Hoyazo is reconstructed in Fig. 5. It is apparent that the development of the Spl-Crd-Kfs coronas replacing garnet is the result of a decompressional event, similar to some regionally metamorphosed granulites (e.g. Hand *et al.*, 1992; Whittington *et al.*, 1998). However, as published grids (e.g. Cenki *et al.*, 2002; Riesco *et al.*, 2004) report Spl-Crd-forming reactions with a positive slope in *P–T* space, decompression should not be considered a rule. For example, available *P–T* data from the rocks of Mazarrón, in which pressure appears to be almost constant at 4.0–4.5 kbar, would suggest heating, rather than decompression, as the cause of corona development.

After a short residence at a relatively shallow depth, which caused the formation of the coronas, the xenoliths were brought to the surface and their HT association 'quenched' during submarine extrusion.

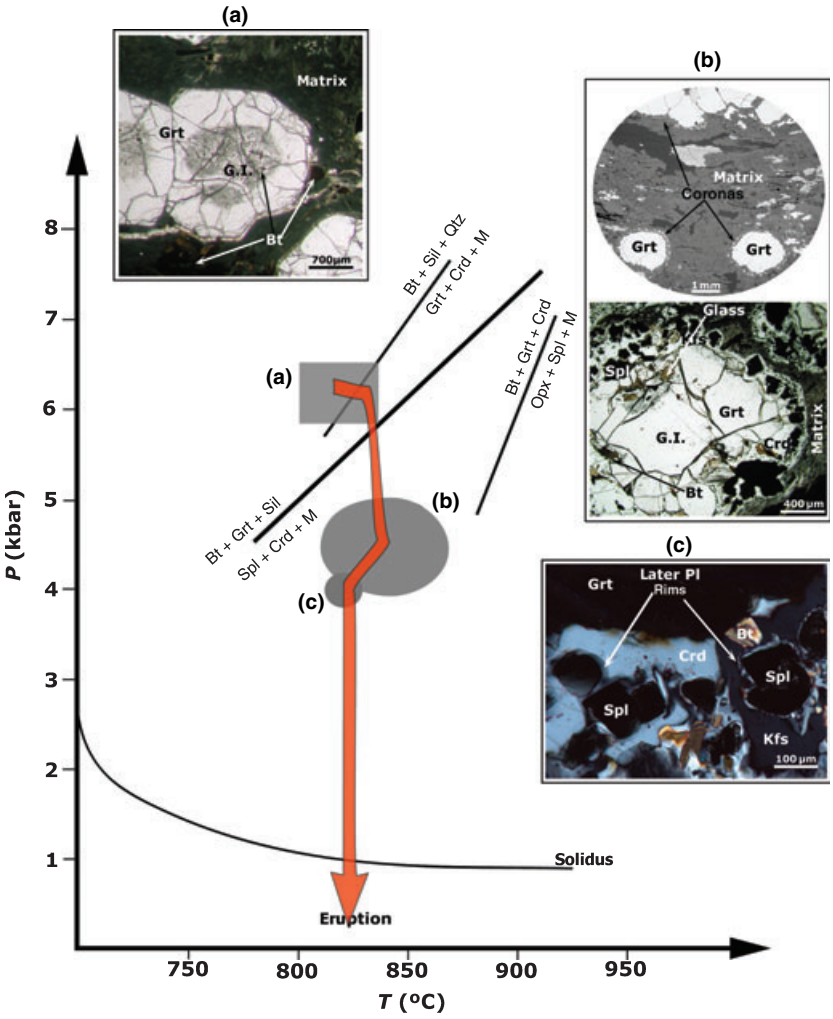

Fig. 5. *P–T* path (red arrow) and representative pictures of corona evolution in a *P–T* diagram for the K_2O-FeO-MgO-Al_2O_3-SiO_2-H_2O (KFMASH) system assuming Kfs in excess. Melting curve is after Carrington & Harley (1995). The three univariant reaction slopes are an average taken from Cenki *et al.* (2002) and Riesco *et al.* (2004). Part figure (a) corresponds to Grt formation at ~850 °C and 6 kbar at El Hoyazo (first melting stage) in Grt-Bt-Sil xenoliths (Cesare *et al.*, 1997), before crossing into the Spl-Crd stability field. Part figure (b) corresponds to the coronitic reaction at ~820 °C, 4.5 kbar, at El Hoyazo (later decompressional melting stage). Part figure (c) (crossed polars) shows an example of Pl rims separating the spinel crystals from the rest of the coronitic phases. This suggests that the Pl rims are later or simultaneous than the Spl-Kfs-Crd-glass corona developed.

At El Hoyazo, the rapid cooling of the xenoliths after eruption of the host dacite could be represented by the very thin plagioclase rims around spinel in the coronas (see Fig. 1c–e). Another possibility is that these late Pl rims are the result of a slight cooling which pre-dates uprise and eruption. This possibility also applies to the Bt-Pl symplectic intergrowths which replace garnet in the xenolith of Mazarrón (Fig. 2f). Therefore, in the *P–T* path of Fig. 5 we have tentatively modelled the post-corona evolution by adding a small event of cooling before eruption (stage c).

The microstructural and thermobarometric study of this work sustains the possibility that, after crustal melting, a small volume of the anatectic dacitic lava hosting the xenoliths has been transferred to shallower crustal levels, where it stagnated before final eruption (Álvarez-Valero, 2004; Álvarez-Valero *et al.*, 2005). Our results also indicate that the two xenolith suites (El Hoyazo and Mazarrón) did not share the same *P–T* evolution before the corona development. Finally, the NCKFMASH mass balance of the coronitic reaction is an example of a chemical approach that takes textural analysis one step further, thus providing more details on the petrogenetic evolution.

ACKNOWLEDGEMENTS

We express our gratitude to M.T. Gómez-Pugnaire for discussion and field assistance, and G. Godard for teaching how to elaborate elemental maps with MultiSpec©. We thank referees T. Johnson and D. Waters for their thoughtful comments and detailed criticism, which helped to clarify the manuscript. Careful editorial handling by M. Brown is gratefully acknowledged. A-V also thanks A. Cabrera and E. Cantalejo for computational facilities at the University of Medicine in Sevilla. This work has been made possible thanks to the support of 01-LEC-EMA22F 'WESTMED – Imaging the Western Mediterranean Margins: A Key Target to Understand the Interaction between Deep and Shallow Processes' Project by the European Science Foundation under the EUROCORES Programme EUROMARGINS, through contract No. ERAS-CT-2003-980409 of the European Commission, DG.

REFERENCES

Álvarez-Valero, A. M., 2004. Petrographic and Thermodynamic Study of the Partial Melting of Restitic Xenoliths from the Neogene Volcanic Province of SE Spain. PhD Thesis, University of Padova, Italy, pp. 223.

Álvarez-Valero, A. M., Cesare, B. & Kriegsman, L. M., 2005. Formation of elliptical garnets in a metapelitic enclave by melt-assisted dissolution and reprecipitation. *Journal of Metamorphic Geology*, **23,** 65–74.

Benito, R., López-Ruiz, J., Cebriá, J. M. *et al*., 1999. Sr and O isotope constraints on source and crustal contamination in the high-K calc-alkaline and shoshonitic Neogene volcanic rocks of SE Spain. *Lithos*, **46,** 773–802.

Carrington, D. P. & Harley, S. L., 1995. Partial melting and phase relations in high-grade metapelites: an experimental petrogenetic grid in KFMASH system. *Contributions to Mineralogy and Petrology*, **120,** 270–291.

Carrington, D. P. & Watt, G. R., 1995. A geochemical and experimental study of the role of K-feldspar during water-undersaturated melting of metapelites. *Chemical Geology*, **122,** 59–76.

Cenki, B., Kriegsman, L. M. & Braun, I., 2002. Melt-producing and melt-consuming reactions in anatectic granulites: P-T evolution of the Achankovil cordierite gneisses, South India. *Journal of Metamorphic Geology*, **20,** 543–561.

Cesare, B., 1999. Multi-stage pseudomorphic replacement of garnet during polymetamorphism: 2. Algebraic analysis of mineral assemblages. *Journal of Metamorphic Geology*, **17,** 735–746.

Cesare, B., 2000. Incongruent melting of biotite to spinel in a quartz-free restite at El Joyazo (SE Spain): textures and reaction characterization. *Contributions to Mineralogy and Petrology*, **139,** 273–284.

Cesare, B. & Gómez-Pugnaire, M. T., 2001. Crustal melting in the Alboran Domain: constraints from enclaves of the Neogene Volcanic Province. *Physics & Chemistry of the Earth*, **26,** 255–260.

Cesare, B. & Maineri, C., 1999. Fluid-present anatexis of metapelites at El Joyazo (SE Spain): constraints from raman spectroscopy of graphite. *Contributions to Mineralogy and Petrology*, **135,** 41–52.

Cesare, B., Salvioli Mariani, E. & Venturelli, G., 1997. Crustal anatexis and melt extraction during deformation in the restitic enclaves at El Joyazo (SE Spain). *Mineralogical Magazine*, **67,** 15–27.

Cesare, B., Marchesi, C., Hermann, J. & Gomez-Pugnaire, M. T., 2003a. Primary melt inclusions in andalusite from anatectic graphitic metapelites: implications for the position of the Al_2SiO_5 triple point. *Geology*, **31,** 573–576.

Cesare, B., Gómez-Pugnaire, M. T. & Rubatto D., 2003b. Residence time of S-type anatectic magmas beneath the Neogene Volcanic Province of SE Spain: a zircon and monazite SHRIMP study. *Contributions to Mineralogy and Petrology*, **146,** 28–43.

Cesare, B., Cruciani, G. & Russo U., 2003c. Hydrogen deficiency in Ti-rich biotite from anatectic metapelites (El Joyazo - SE Spain): crystal-chemical aspects and implications for high-temperature petrogenesis. *American Mineralogist*, **88,** 583–595.

Chakraborty, S. & Ganguly, J., 1991. Compositional zoning and cation diffusion in aluminosilicate garnets. In: *Diffusion, Atomic Ordering and Mass Transport – Selected Problems in Geochemistry. Advances in Physical Geochemistry* (ed. Ganguly, J.), vol. 8, 120–170 Springer, Berlin.

Corona-Chávez, P., Poli, S. & Bigioggero, B., 2006. Syn-deformational migmatites and magmatic-arc metamorphism in the Xolapa Complex, Southern Mexico. *Journal of Metamorphic Geology*, **24,** 169–191.

Day, H. W. & Springer, R. K., 2005. First appearance of actinolite in the prehnite-pumpellyite facies, Sierra Nevada, California. *The Canadian Mineralogist*, **43,** 89–104.

Duggen, S., Hoernle, K., Van Den Bogaard, P. & Harris C., 2004. Magmatic evolution of the Alboran region: the role of subduction in forming the western Mediterranean and causing the Messinian Salinity Crisis. *Earth and Planetary Science Letters*, **218,** 91–118.

Fernández-Soler, J. M., 1996. El volcanismo calco-alcalino en el parque natural de Cabo de Gata-Níjar (Almería). Estudio Volcanológico y Petrológico. *Sociedad Almeriense de Historia Natural. Monografías del Medio Natural*, **2,** 1–295.

Ferry, J. M. & Spear, F. S., 1978. Experimental calibration of the partitioning of Fe and Mg between biotite and garnet. *Contributions to Mineralogy and Petrology*, **66,** 113–117.

Fisher, G. W., 1989. Matrix analysis of metamorphic mineral mineral reactions. As calculated mass balances contain assemblages and reactions. *Contributions to Mineralogy and Petrology*, **102,** 69–77.

Greenwood, H. J., 1967. The N-dimensional tie-line problem. *Geochimica et Cosmochimica Acta*, **31,** 465–490.

Hand, M., Dirks, P. H. G. M., Powell, R. & Buick, I. S., 1992. How well established is isobaric cooling in Proterozoic orogenic belts? An example from the Arunta inlier, central Australia. *Geology*, **20,** 649–652.

Hand, M., Scrimgeour, I., Powell, R., Stüwe, K. & Wilson, C. J. L., 1994. Metapelitic granulites from Jetty Peninsula, east Antarctica: formation during a single event or by polymetamorphism? *Journal of Metamorphic Geology,* **12,** 557–573.

Harley, S. L. & Carrington, D. P., 2001. The distribution of H_2O between cordierite and granitic melt; H_2O incorporation in cordierite and its application to highgrade metamorphism and crustal anatexis. *Journal of Petrology*, **42,** 1595–1620.

Hartel, T. H. D. & Pattison, D. R. M., 1996. Genesis of the Kapuskasing (Ontario) migmatitic mafic granulites by dehydration melting of amphibolite: the importance of quartz to reaction progress. *Journal of Metamorphic Geology*, **14,** 591–611.

Hodges, K. V. & Crowley, P. D., 1985. Error estimation in empirical geothermometry and geobarometry for pelitic systems. *American Mineralogist*, **70,** 702–709.

Holdaway, M. J., 2000. Application of new experimental and garnet Margules data to the garnet–biotite geothermometer. *American Mineralogist*, **85,** 881–892.

Holdaway, M. J. & Lee, S. M., 1977. Fe-Mg cordierite stability in high grade pelitic rocks based on experimental, theorical and natural observations. *Contributions to Mineralogy and Petrology*, **63,** 175–198.

Hollister, L. S., 1977. The reaction forming cordierite from garnet, the Khtada Lake Metamorphic Complex, British Columbia. *Canadian Mineralogist*, **15,** 217–229.

Ings, S. J. & Owen, J. V., 2002. 'Decompressional' reaction textures formed by isobaric heating: an example from the thermal aureole of the Taylor Brook Gabbro Complex, western Newfoundland. *Mineralogical Magazine*, **66,** 941–951.

Johnson, T., Brown, M., Gibson, R. & Wing, B., 2004. Spinel–cordierite symplectites replacing andalusite: evidence for melt-assisted diapirism in the Bushveld Complex, South Africa. *Journal of Metamorphic Geology*, **22,** 529–545.

Koziol, A. M., 1989. Recalibration of the garnet–plagioclase–Al_2SiO_5–quartz (GASP) geobarometer and applications to natural parageneses. *EOS Trans. American Geophysical Union*, **70,** 493.

Koziol, A. M. & Newton, R. C., 1988. Redetermination of the anorthite breakdown reaction and improvement of the plagioclase–garnet–Al_2SiO_5–quartz geobarometer. *American Mineralogist*, **73,** 216–223.

Kretz, R., 1983. Symbols for rock-forming minerals. *American Mineralogist*, **68,** 277–279.

Kriegsman, L. M., 2001. Partial melting, partial melt extraction and partial back reaction in anatectic migmatites. *Lithos*, **56,** 75–96.

Kriegsman, L. M. & Hensen, B. J., 1998. Back reaction between restite and melt: implications for geothermobarometry and pressure-temperature paths. *Geology*, **26,** 1111–1114.

López-Ruiz, J. & Rodríguez-Badiola, E., 1980. La region volcanica Neogena del sureste de España. *Estudios de Geología*, **36,** 5–63.

McDade, P. & Harley, S. L., 2001. A petrogenetic grid for aluminous granulite facies metapelites in the KFMASH system. *Journal of Metamorphic Geology*, **19,** 45–59.

Mezger, J. E., Chacko, T. & Erdmer, P., 2001. Metamorphism along a late Mesozoic accretionary continental margin: a case study from the northern Coast Belt of the North American Cordillera. *Journal of Metamorphic Geology*, **19,** 121–138.

Morgan, G. B. & London, D., 1996. Optimizing the electron microprobe analysis of hydrous alkali aluminosilicate glasses. *American Mineralogist*, **81,** 1176–1185.

Nekvasil, H. & Burnham, C. W., 1987. The calculated individual effects of pressure and water content on phase equilibiria in the granite system. In: *Magmatic Processes: Physicochemical Principles* (ed. Mysen, B.O.), pp. 433–445. Geochemical Society, University Park, PA.

Passchier, C. W. & Trouw, R. A. J., 1996. *Microtectonics*. Springer-Verlag, Heidelberg, pp. 289.

Pattison, D. R. M., 1992. Stability of andalusite and sillimanite and the Al2SiO5 triple point: constraints from the Ballachulish aureole, Scotland. *Journal of Geology*, **100,** 423–446.

Perchuk, L. L., Gerya, T. V. & Nozhkin, A. D., 1989. Petrology and retrogression in granulites of the Kanskiy Formation, Yenisey Range, Eastern Siberia. *Journal of Metamorphic Geology*, **7,** 599–617.

Platt, J. P. & Vissers, R. L. M., 1989. Extensional collapse of thickened continental lithosphere: a working hypothesis for the Alborán Sea and Gibraltar arc. *Geology*, **17,** 540–543.

Pouchou, J. L. & Pichoir, F., 1984. Un nouveau modèle de calcul pour la microanalise quantitative par spectrométrie de rayon-X: I. Application à l'analyse d'échantillons homogènes. *La Recherche Aérospatiale*, **3,** 167–192.

Riesco, M., Stüwe, K., Reche, J. & Matínez, J., 2004. Silica depleted melting of pelites. Petrogenetic grid and application to the Susqueda Aureole, Spain. *Journal of Metamorphic Geology*, **22,** 475–494.

Storm, L. C. & Spear, F. S., 2005. Pressure, temperature and cooling rates of granulite facies migmatitic pelites from the southern Adirondack Highlands, New York. *Journal of Metamorphic Geology*, **23,** 107–130.

Taylor, S. R. & McLennan, S. M., 1985. *The Continental Crust: Its Composition and Evolution*. Blackwell, Oxford, pp. 307.

Thompson, A. B., 1976. Mineral reactions in pelitic rocks: I. Prediction of P-T-X (Fe-Mg) phase relations. *American Journal of Science*, **276,** 401–424.

Topuz, G., Altherra, R., Kalta, A., Satırb, M., Wernera, O. & Schwarza W. H., 2004. Aluminous granulites from the Pulur complex, NE Turkey: a case of partial melting, efficient melt extraction and crystallisation. *Lithos*, **72,** 183–207.

Torres-Roldán, R. L., García-Casco, A. & García-Sánchez, P. A., 2000. CSpace: an integrated workplace for the graphical and algebraic analysis of phase assemblages on 32-bit Wintel platforms. *Computers and Geosciences*, **26,** 779–793.

Turner, S. P., Platt, J. P., George, R. M. M., Kelley, S. P., Pearson, D. G. & Nowell G. M., 1999. Magmatism associated with orogenic collapse of the Betic-Alboran Domain, SE Spain. *Journal of Petrology*, **40,** 1011–1036.

Vernon, R. H., 1996. Problems with inferring *P-T-t* paths in low-*P* granulite facies rocks. *Journal of Metamorphic Geology*, **14,** 143–153.

Vernon, R. H., 2004. *A Practical Guide to Rock Microstructure*. Cambridge University Press, Cambridge, pp. 594.

Vielzeuf, D. & Montel, J. M., 1994. Partial melting of metagreywackes. Part 1. Fluid-absent experiments and phase relationships. *Contributions to Mineralogy and Petrology*, **117,** 375–393.

Vissers, R. L. M., Platt, J. P. & Van Der Wal D., 1995. Late orogenic and compositional constraints on 'post orogenic' magmatism. Geology extension of the Betic Cordillera and the Alborán Domain: a lithospheric view. *Tectonics*, **14,** 786–803.

White, R. W. & Powell, R., 2002. Melt loss and the preservation of granulite facies mineral assemblages. *Journal of Metamorphic Geology*, **20,** 621–632.

White, R. W., Powell, R. & Holland, T. J. B., 2001. Calculation of partial melting equilibria in the system Na_2O-CaO-K_2O-FeO-MgO-Al_2O_3-SiO_2-H_2O (NCKFMASH). *Journal of Metamorphic Geology*, **19,** 139–153.

White, R. W., Powell, R. & Clarke, G. L., 2002. The interpretation of reaction textures in Fe-rich metapelitic granulites of the Musgrave Block, central Australia: constraints from mineral equilibria calculations in the system K_2O-FeO-MgO-Al_2O_3-SiO_2-H_2O-TiO_2-Fe_2O_3. *Journal of Metamorphic Geology*, **20,** 41–55.

White, R. W., Powell, R. & Clarke, G. L., 2003. Prograde metamorphic assemblage evolution during partial melting of metasedimentary rocks at low pressures: migmatites from Mt Stafford, Central Australia. *Journal of Petrology*, **44,** 1937–1960.

Whittington, A., Harris, N. & Baker, J., 1998. Low-pressure crustal anatexis. In: *What Drives Metamorphism and Metamorphic Reactions? Special Publication 138* (eds Treolar, P. J. & O'Brien, P. J.), pp. 183–198. Geological Society, London.

Zeck, H. P., 1968. Anatectic Origin and Further Petrogenesis of Almandine-bearing Biotite Cordierite-labradorite-dacite with many Inclusions of Restite and Basaltoid Material, Cerro de Hoyazo, SE Spain. PhD Thesis, University of Amsterdam, Netherlands.

Zeck, H. P., 1970. An erupted migmatite from Cerro de Hoyazo, SE Spain. *Contributions to Mineralogy and Petrology*, **26,** 225–246.

Zeck, H. P. & Williams, I. S., 2002. Inherited and magmatic zircon from Neogene Hoyazo cordierite dacite, SE Spain-Anatectic source rock provenance and magmatic evolution. *Journal of Petrology*, **43,** 1089–1104.

Zeck, H. P., Kristensen, A. B. & Williams I. S., 1998. Post-collisional volcanism in a sinking slab setting–crustal anatectic origin of pyroxene-andesite magma, Caldear Volcanic Group, Neogene Alborán volcanic Province, southeastern Spain. *Lithos*, **45,** 499–522.

Received 24 April 2006; revision accepted 23 November 2006